České vysoké učení technické v Praze
Fakulta jaderná a fyzikálně inženýrská

Czech Technical University in Prague
Faculty of Nuclear Sciences and Physical Engineering

Doc.Dr.Ing. Michal Beneš

Nelineární difuze a její aplikace

Nonlinear Diffusion and Applications

Summary

The diffusion processes are described by the parabolic partial differential equations thoroughly studied mathematically and widely applied in thermodynamics, electricity, chemistry, porous media, biology or economics. The heat-conduction/diffusion equation has been exploring the principle of the closest-neighbor interaction leading to the use of the Laplace operator in the simplest setting, and as the conservation law, to the use of gradient expressions for the flux of the investigated quantity. Recently, yet another role of the solution became important - the motion of the solution level sets. In the nonlinear laws, they can represent the phase interfaces, evolving patterns or object boundaries.

In this text, the framework of nonlinear diffusion is presented. For this purpose, the results obtained in the domain of reaction-diffusion equations appearing in chemistry and combustion in particular are discussed. In this case, the rich spatio-temporal dynamics is the consequence of competitive interaction of the reactive and diffusive processes. The results obtained in modelling of microstructure growth in solidification, thin-layer dynamics and material-defect dynamics belong to the domain of material science. Here, the moving material boundaries are described by nonlinear evolution laws. The nonlinear diffusion is currently used in the computer image processing as well, as shown in the result describing the heart left-ventricle segmentation in the images obtained by the magnetic resonance. In several presented examples, the common evolution law for an interface can be found. It links the interface normal velocity, the mean curvature and the external force together. The generalization of diffusion processes by means of the fractional dispersion and advection is sketched in the last example.

The rich variety of features and applications therefore make the nonlinear diffusion laws the interesting subject of current and future research.

Souhrn

Difuzní procesy jsou popsány parabolickými parciálními diferenciálními rovnicemi, které jsou důkladně prostudovány matematicky a široce použity v oblasti termodynamiky, elektřiny, chemie, porézního prostředí, biologie nebo ekonomie. Rovnice vedení tepla či difuzní rovnice využívá interakce prostorově sousedících hodnot řešení, která je v nejjednodušší podobě popsána Laplaceovým operátorem. Jako zákon zachování rovnice používá vyjádření toku zkoumané veličiny pomocí jejího gradientu. Mezi moderní role této rovnice patří využití pohybu vrstevnic jejího řešení, které v nelineárních případech mohou představovat fázová rozhraní, měnící se obrazce nebo hranice objektů.

Tato práce se zabývá problematikou nelineární difuze. Představuje výsledky získané v oblasti reakčně-difuzních rovnic popisujících chemické reakce a procesy spalování. V tomto případě je bohatá prostoročasová dynamika důsledkem interakce reakčních a difuzních procesů. Do oblasti materiálových věd míří další zmíněné výsledky - modelování růstu mikrostruktur při tuhnutí, dynamiky tenkých vrstev a materiálových poruch. Pohyblivá materiálová rozhraní jsou popsána nelinárními zákony. Stejně tak je nelineární difuze používána v oblasti počítačového zpracování obrazu, kam patří ukázka segmentace levé srdeční komory ve snímcích získaných magnetickou rezonancí. V několika z uvedených oblastí se přitom používá stejný zákon pohybu pro pohyblivá rozhraní, který dává do vztahu normálovou rychlost rozhraní, jeho střední křivost a vnější silové působení.

Nelineární difuze tedy díky svým rozmanitým vlastnostem a použití zůstává zajímavým předmětem současného a budoucího výzkumu.

Klíčová slova: nelineární difuze, reakčně-difuzní systémy, fázové přechody, pohyb podle střední křivosti, povrchová difuze, dislokace, vrstevnicová rovnice, anomální difuze

Keywords: nonlinear diffusion, reaction-diffusion systems, phase transitions, motion by mean curvature, surface diffusion, dislocations, level set equation, anomalous diffusion

---

České vysoké učení technické v Praze

Název: Nelineární difuze a její aplikace
Autor: Michal Beneš
Počet stran 34
Náklad:

ISBN

Contents

1 Introduction

The diffusion partial differential equation occupies a unique position in modern applied mathematics and physics. Since its primary derivation in the work of J.B.J. Fourier dating back to 1807 and 1822, it is used to describe the heat transfer by conduction in physical systems, but it also arises in many other fields such as electricity, chemical diffusion, fluids in porous media, biology and economics.

When using of the linear form of the heat conduction or diffusion equation it became clear that despite of its key role in the theory of equations of mathematical physics it represents an approximative model. The thermodynamical context, dependence of the physical parameters on the solution, or complexity of some applications such as multi-phase porous media flow or image processing make the diffusion-type balance law intrinsically non-linear.

We therefore devote this text to a brief summary of knowledge which was gathered during studies of various non-linear diffusion phenomena arising in the dynamics of chemical reactions, in solid-liquid phase transitions, thin-film evolution and defect dynamics in materials, and in the processing of images by the evolution partial differential equations. In this way we try to provide the reader with a comparison of the discussed diffusion processes, with a notion of mathematical and numerical tools used for their analysis, and also with the impression of further development in their investigation.

The genesis of the diffusion equation and domains it influenced during more than two hundred years of its knowledge are more than remarkable and are linked to the developments of many scientists since Fahrenheit, Laplace, Fourier, Ohm, Thomson, Fick Poiseuille, Darcy, Einstein, Richards, Fermi to the contemporary mathematicians and physicists. The problems we mention confirm this line and indicate new aspects which appeared recently. The origin of the equation is related to the concept of the closest-neighbor dependence (of temperature, in particular) leading to the derivation of the Laplace operator. Later, and also in other contexts such as in porous media, this approach was connected to the concentration or pressure drop providing the flux of the investigated quantity. Finally, the randomly behaving systems (particles, but also errors, species or stock prices) were found to follow the rules provided by the original heat conduction law. Departure from the concept of the Brownian motion and the Gaussian distribution can open new perspectives such as study of anomalies in variety of transport problems.

2 Concept of nonlinear diffusion

The limited scope of the text covers the nonlinear diffusion processes described by the following abstract evolution law

$$\begin{aligned} \frac{dU}{dt} + \mathbf{A}(U) &= \mathbf{F}(U), \\ U|_{t=0} &= U_{ini}. \end{aligned} \tag{1}$$

in the Hilbert space $\mathbf{H}$ with the scalar product $(\cdot,\cdot)$ and the norm $\|\cdot\|$. The solution U is a map from $(0,T)$ to a suitable subset of $\mathbf{H}$. The basic setting assumes that the operator $\mathbf{A}$ is linear self-adjoint unbounded in $\mathbf{H}$ with $D(\mathbf{A})$ dense in $\mathbf{H}$, positive closed and with $\mathbf{A}^{-1}$ compact. We set $\mathbf{V} = D(\mathbf{A}^{\frac{1}{2}})$ with the norm $\|\cdot\|_V$. Several nonlinear generalizations related to $\mathbf{A}$ are considered. The nonlinear mapping $\mathbf{F}$ is from $\mathbf{H}$ to $\mathbf{H}$. The evolution law requires the initial state to be described (U_{ini}).

Law (1) originates in the conservation law of the quantity U as shown in the following example.

Example. For the sake of simplicity, consider a reaction occurring in a one-dimensional tank $(0, L)$ of the length L. If x is the spatial variable, and u denotes the concentration of the only species influenced, the conservation of u reads as:

$$\frac{\partial u(t,x)}{\partial t} + \frac{\partial j(t,x)}{\partial x} = f(u(t,x)),$$

where f describes the reaction source term, j is the concentration flux. If the linear Fick law is accepted for the concentration flux ($D > 0$)

$$j(t,x) = -D\frac{\partial u(t,x)}{\partial x},$$

we obtain the simple example of law (1) in the form of a scalar reaction-diffusion equation. The operator $\mathbf{A}(U) = -D\frac{\partial^2 u(t,x)}{\partial x^2}$ can be linked to the boundary conditions, e.g. of the Dirichlet type ($u(t,0) = u(t,L) = 0$), and $\mathbf{F}(U) = f(u)$. In this case $\mathbf{H} = \mathrm{L}_2(\Omega)$ and $\mathbf{V} = \mathrm{H}_0^{(1)}(\Omega)$.

In the subsequent text, we observe that the quantity U can become vector-valued and, due to complexity of physical processes considered, the diffusion operator $\mathbf{A}$ and the term $\mathbf{F}$ become nonlinear.

2.1 Mathematics of nonlinear diffusion

The key issues of mathematical analysis are related to the existence, uniqueness and parameter dependence of the diffusion problems. The desired results are usually obtained by means of the compactness and monotonicity methods (see [27, 60]) using the apriori estimates, maximum principle and invariant regions (see [57]). The nonlinearity in the diffusion operators is frequently given by the anisotropy of the diffusion controlled by the solution gradient. This allows to explore the monotonicity method. Nonlinear terms depending on the solution gradient require additional techniques (see [15]). In some cases, the framework of the viscosity solution can be applied ([22]). Naturally, each of the particular problems exhibits its own special features with special difficulties of the mathematical treatment.

In the following, we describe main line of mathematical analysis for the given framework.

Apriori estimates. For problem (1), the weak formulation can be formally obtained as follows

$$\begin{aligned} \frac{d}{dt}(U,V) + (\mathbf{A}(U),V) &= (\mathbf{F}(U),V), \text{ in } \mathcal{D}'(0,T) \text{ for each } V \in \mathbf{V}, \\ U|_{t=0} &= U_{ini}. \end{aligned} \tag{2}$$

The solution estimates can be obtained by formally testing (2) (through the expansion of the solution by means of a linear basis of $\mathbf{V}$) by the solution U:

$$\frac{1}{2}\frac{d}{dt}\|U\|^2 + (\mathbf{A}(U),U) = (\mathbf{F}(U),U),$$

or by testing by the time derivative $\frac{dU}{dt}$ obtaining:

$$\|\frac{dU}{dt}\|^2 + (\mathbf{A}(U),\frac{dU}{dt}) = (\mathbf{F}(U),\frac{dU}{dt}),$$

Depending on the problem nature, the classical or the weak maximum principle can be adopted, or its vectorial analogue - the invariant regions method can be used. For the definition of the invariant region $\mathcal{O}$ for the values of the solution U and its use, see [57, 55] and references therein.

Approximate solutions. Exploring the finite-dimensional subspace $\mathbf{V}_h$ of $\mathbf{V}$ we find the solution of the finite-dimensional problem

$$\begin{aligned} \frac{d}{dt}(U_h, V) + (\mathbf{A}(U_h), V) &= (\mathbf{F}(U_h), V), \text{ for each } V \in \mathbf{V}_h, \\ U_h|_{t=0} &= \mathcal{P}_h U_{ini}. \end{aligned}$$

where $\mathcal{P}_h$ is the projector on $\mathbf{V}_h$.

This problem usually possesses a unique solution on a time interval $(0, T_h)$ guaranteed by the theory of ordinary differential equations. The mentioned apriori estimates unify the extent of the time variable to $(0, T)$.

Convergence. The mentioned approximate solutions U_h are bounded in suitable spaces due to the apriori estimates when $h \to 0_+$. The convergence in terms $\mathbf{A}(U_h), V)$ and $(\mathbf{F}(U_h), V)$ is achieved due to particular properties of the mapping $\mathbf{A}$ - e.g. monotonicity and further detailed features, and of the mapping $\mathbf{F}$ - the simplest of them is the Lipschitz continuity.

Uniqueness. Typically, two solutions U_1 and U_1 of (2) are assumed and the weak equalities are subtracted to get

$$\begin{aligned} \frac{d}{dt}(U_1 - U_2, V) + (\mathbf{A}(U_1) - \mathbf{A}(U_2), V) &= (\mathbf{F}(U_1) - \mathbf{F}(U_2), V), \text{ for each } V \in \mathbf{V}, \\ U_1|_{t=0} - U_2|_{t=0} &= 0. \end{aligned}$$

The properties of $\mathbf{A}$ and of $\mathbf{F}$ (e.g. Lipschitz continuity) help to obtain (via the Gronwall argument) uniqueness. In special cases, the error estimates for the approximate solution U_h, and the parameter dependence of the solution can be obtained in a similar way.

Remark. Corresponding detailed results are claimed in sections devoted to the particular examples of the nonlinear diffusion.

2.2 Numerical methods for nonlinear diffusion

Each of approaches to the numerical solution of the problem (1) performs the discretization in time and space simultaneously or subsequently.

The **Rothe method** of time discretization produces a sequence of stationary problems at given time levels. Denoting $\tau > 0$ the time step and $U^{(k)} = U(k\tau),\ k = 0, \ldots, N_T$ we derive:

- the **explicit Euler scheme** ($k = 0, \ldots, N_T - 1$):

$$\frac{U^{(k+1)} - U^{(k)}}{\tau} + \mathbf{A}(U^{(k)}) = \mathbf{F}(U^{(k)}), \quad U^{(0)} = U_{ini},$$

- the **implicit Euler scheme** ($k = 0, \ldots, N_T - 1$):

$$\frac{U^{(k+1)} - U^{(k)}}{\tau} + \mathbf{A}(U^{(k+1)}) = \mathbf{F}(U^{(k+1)}), \quad U^{(0)} = U_{ini},$$

  or the semi-implicit version with $\mathbf{F}(U^{(k)})$.

The **method of lines** generates the spatial discretization ($\mathbf{A}_h$, $\mathbf{F}_h$, U_h are spatial discretizations of $\mathbf{A}$, $\mathbf{F}$, U) prior to the time discretization.

$$\begin{aligned} \frac{dU_h}{dt} + \mathbf{A}_h(U_h) &= \mathbf{F}_h(U_h) \text{ pro } t \in (0,T), \\ U_h|_{t=0} &= \mathcal{P}_h U_{ini}. \end{aligned}$$

The resulting system of ODEs can be solved by corresponding time solver such as one of the Runge-Kutta methods.
The **spatial discretizations** usually explore the following methods:

- the **Finite-Difference Method** assumes availability of the discrete, possibly uniform set of nodes $\bar{\omega}_h \subset \bar{\Omega}$ at which the differential expressions in (1) are replaced by the difference expressions. In described applications, the approximate solution is a map with values in some finite-dimensional Banach space of the grid functions $\mathcal{H}_h$ (maps of $\bar{\omega}_h$ to $\mathbb{R}$)

  $$U^h : \langle 0, T\rangle \to \mathcal{H}_h \text{ or } U^h : \{0, \ldots, N_T\} \to \mathcal{H}_h$$

  according to the discretization in time. The original problem is replaced by a system of nonlinear equations for U^h as the unknown. The gradient differential operator ∇ is approximated by $\bar{\nabla}_h$ - the backward difference operator, the divergence operator by ∇_h - the forward difference operator, and the Laplace operator Δ by the second-order central-difference operator Δ_h in arbitrary spatial dimension.

- the **Finite-Volume Method** has the same philosophy as the previous method. However, the piece-wise integration over the finite volumes as parts of Ω precedes the approximation of differential expressions in order to keep the balance principle at the discrete level as well.

- the **Galerkin method** - sometimes in combination with other methods - explores the existence of the orthonormal basis $\{v_j\}_{j=0}^{\infty}$ of the space $\mathbf{V}$. Using only m of them for defining the approximative solution: $U^m = \sum_{i=1}^{m} \gamma_i^m v_i$ in such a way that

  $$\begin{aligned} \frac{dU^m}{dt} + \mathbf{A}(U^m) &= \mathbf{F}(U^m) \text{ in } \mathcal{P}_m \mathrm{V}, \\ U^m\,|_{t=0} &= \mathcal{P}_m U_{ini}, \end{aligned}$$

  where $\mathcal{P}_m$ is projector into $[v_1, \ldots, v_m]_\lambda$.

- the **nonlinear Galerkin method.** Similar to the Galerkin method, it uses the orthonormal basis $\{v_j\}_{j=0}^{\infty}$ of the space $\mathbf{V}$. It looks for the solution approximation U^m and its correction Z^m in the form: $U^m = \sum_{i=1}^{m} \gamma_i^m v_i,\ Z^m = \sum_{i=m+1}^{M} \delta_i^m v_i,\ M > m$ in such a way that

  $$\begin{aligned} \frac{dU^m}{dt} + \mathbf{A}(U^m) &= \mathbf{F}(U^m + Z^m) \text{ in } \mathcal{P}_m \mathrm{V}, \\ \mathbf{F}(U^m) - \mathbf{A}(Z^m) + \mathbf{F}'(U^m) Z^m &= 0 \text{ in } \mathcal{P}_M \mathrm{V} - \mathcal{P}_m \mathrm{V}, \\ U^m\,|_{t=0} &= \mathcal{P}_m u_0, \end{aligned}$$

  where $\mathcal{P}_M$ projects onto $[v_1, \ldots, v_M]_\lambda$ and where we assumed that $\mathbf{A}$ is linear, for simplicity. As the advantage, the approximation converges in some sense on $(0, +\infty)$. The correction Z^m of U^m tends to 0 when $m \to +\infty$.

We sketch the methods of numerical analysis for the mentioned approaches and assume for simplicity, that $\mathbf{A}$ is linear.

Numerical analysis of the implicit scheme. The scheme has the following form

$$\begin{aligned} U_{\bar{t}}^{(k+1)} + \mathbf{A}(U^{(k+1)}) &= \mathbf{F}(U^{(k+1)}),\ k = 0, \ldots, N_T - 1, \\ U^{(0)} &= U_{ini}, \end{aligned} \tag{3}$$

where $U_{\bar{t}}^{(k)} = \frac{1}{\tau}(U^{(k)} - U^{(k-1)})$. The properties of $\mathbf{A}$ imply the scalar product on $\mathbf{V}$ as

$$(U, V)_A \stackrel{\text{def}}{=} (\mathbf{A}U, V),$$

which can be used in the energy inequalities. We formally multiply (3) by the difference $U_{\bar{t}}^{(k)}$, and get

$$\|U_{\bar{t}}^{(k+1)}\|^2 + (U^{(k+1)}, U_{\bar{t}}^{(k+1)})_A = (\mathbf{F}(U^{(k+1)}), U_{\bar{t}}^{(k+1)}).$$

For simplicity, we explore the boundedness of $\mathbf{F}$ by a constant $F > 0$, and the Lipschitz continuity, we obtain

$$\sum_{k=1}^{l} \tau \|U_{\bar{t}}^{(k)}\|^2 + \|U^{(l)}\|_A^2 - \|U^{(0)}\|_A^2 + \sum_{k=1}^{l} \|U^{(k)} - U^{(k-1)}\|_A^2 \leq F^2 l \tau,$$

from which the apriori estimates for $\|U^{(l)}\|_A^2$ and $\sum_{k=1}^{l} \tau \|U_{\bar{t}}^{(k)}\|^2$ follow.

Defining the Rothe functions ($k = 0, \ldots, N_T$):

$$\begin{aligned} \mathcal{S}_\tau U^{(\tau)}(t) &= U^{(k)},\ \text{pro } t \in ((k-1)\tau, k\tau\rangle, \\ \mathcal{Q}_\tau U^{(\tau)}(t) &= U^{(k-1)} + (t - (k-1)\tau)\frac{U^{(k)} - U^{(k-1)}}{\tau}, \\ &\quad \text{pro } t \in \langle (k-1)\tau, k\tau\rangle, \end{aligned} \tag{4}$$

we can confirm by the limit procedure using the compactness method that the common limit of the Rothe functions becomes the solution of (1).

Numerical analysis of the method of lines represented by the semi-discrete system

$$\begin{aligned} \frac{dU_h}{dt} + \mathbf{A}_h U_h &= \mathbf{F}_h(U_h) \text{ pro } t \in (0, T), \\ U_h|_{t=0} &= \mathcal{P}_h U_{ini} \end{aligned}$$

is again performed by multiplying $\frac{dU_h}{dt}$ and integrating over $\bar{\omega}_h$. The resulting equality is written by means of discretized products in $\mathbf{H}$ a $\mathbf{V}$ denoted by h.

$$\|\frac{dU_h}{dt}\|_h^2 + \frac{1}{2}\frac{d}{dt}\|U_h\|_{A_h}^2 = (\mathbf{F}_h(U_h), \frac{dU_h}{dt})_h,$$

from which

$$\int_0^t \|\frac{dU_h}{dt}\|_h^2 dt + \|U_h\|_{A_h}^2(t) \leq \|U_h\|_{A_h}^2(0) + F^2 t.$$

We define the operators of extrapolation from $\bar{\omega}_h$ on Ω in the analogy to (4): $\mathcal{S}_h$, a $\mathcal{Q}_h$ and use the compact imbedding to obtain the limit in the semi-discrete system.

3 Diffusion in Physical Models

As mentioned above, we provide several examples of nonlinear diffusion arising in reaction kinetics, combustion, solid-liquid phase changes, thin film evolution and dislocation dynamics in crystalline materials, and in computer image processing. The original role of the diffusion equation and of its solution as the conservation law for the corresponding physical quantity using the expression for the quantity flux is enriched by the role of the solution level-sets describing interfaces. This new role found application in the description of moving domains in general.

We refer to our own results as well as to key results obtained for each of particular examples keeping in mind basic knowledge described in many resources of which we can refer e.g. to [60] for general framework of parabolic problems as dynamical systems, [57] for the framework of reaction-diffusion problems, [63] for the framework of the free-boundary problems, [56] for the level-set methods and [48] for an example of historical review on heat conduction.

3.1 Reaction-diffusion systems in chemistry and biology

The origin of the reaction-diffusion systems is described in the example mentioned in Section 2. The reaction-diffusion system has a typical form as follows:

$$\begin{aligned} \frac{\partial c^1}{\partial t} &= D^1 \Delta c^1 + f^1(c^1, \dots, c^n), \\ &\dots \\ \frac{\partial c^n}{\partial t} &= D^n \Delta c^n + f^2(c^1, \dots, c^n), \end{aligned} \tag{5}$$

where $f^1, \dots, f^n$ are the reaction describing polynomial expressions, the unknown functions $c^1, \dots, c^n$ depend on time and space. Denoting

$$\begin{aligned} &U = [c^1, \dots, c^n],\ \mathbf{A}(U) = [D^1 \Delta c^1, \dots, D^n \Delta c^n], \\ &\mathbf{F}(U) = [f^1(c^1, \dots, c^n), \dots, f^n(c^1, \dots, c^n)], \end{aligned}$$

system (5) belongs to the problem class described by (1).

The mathematical analysis of systems (5) can be accomplished using the notion of the invariant region (denoted by $\mathcal{O}$) as suggested in [57] and used in [55, 62, 38]. The existence theorem typically has the following form:

Theorem 1. *Consider system (5) within (1), and let the initial state U_{ini} belongs to $\mathbf{V} = Def(\sqrt{\mathbf{A}})$ and has the values in $\mathcal{O}$ for almost all x, then the unique weak solution of this problem exists on $(0, T)$ for arbitrary $T > 0$ in $\mathrm{L}_2(0, T; \mathbf{V})$.*

Proof follows from [57].

The nonlinear Galerkin scheme applied to system (5) converges due to the following statement

Theorem 2. *Consider system (5) within (1), and let the initial state U_{ini} belonging to $\mathrm{V} = Def(\sqrt{\mathbf{A}})$ has the values in $\mathcal{O}$ for almost all x. Then the sequence $\{U^m\}_{m=1}^{\infty}$ of solutions obtained by the nonlinear Galerkin method strongly converges to the unique solution $U \in \mathrm{L}_2(0,T;\mathbf{V})$ of the original problem in $\mathrm{L}_2(0,T;\mathbf{H})$ for arbitrary $T > 0$, provided $m \to +\infty$ and $M > m$. Furthermore there is a subsequence $\{U_{m'}\}_{m'=1}^{\infty}$ of $\{U_m\}_{m=1}^{\infty}$ converging weak-* to U in $\mathrm{L}_2(0,+\infty;\mathbf{H})$.*

Proof follows from [55].

Here we list several examples we had the opportunity to study. The research was focused on numerical solution accurately approximating rich dynamics of the time evolution.

3.1.1 Gray-Scott model

The first example is the model introduced by P. Gray and S. K. Scott (see [32]). It describes the autocatalytic chemical reaction

$$U + 2V \to 3V, \quad V \to P, \tag{6}$$

where U, V are reactants and P is final product of the reaction. The chemical substance U is being continuously added into the reactor and the product P is being continuously removed from the reactor during the reaction. The model has been extensively studied, e.g., in [25, 38]. This model is well known to exhibit rich dynamics, as shown in [49].

The chemical reaction (6) may be rewritten into a dimensionless form as in [38]. Assume that Ω represents the reactor, where the chemical reaction takes place, $\partial\Omega$ is boundary of Ω and ν is the unit outward normal on Ω. Then the initial-boundary value problem for the Gray-Scott model is the following system:

$$\frac{\partial u}{\partial t} = D_u \Delta u - uv^2 + F(1-u), \tag{7}$$

$$\frac{\partial v}{\partial t} = D_v \Delta v + uv^2 - (F+k)v, \tag{8}$$

in $\Omega \times (0,T)$ with initial conditions

$$u(\cdot,0) = u_{ini}, \quad v(\cdot,0) = v_{ini},$$

and zero Neumann boundary conditions

$$\frac{\partial u}{\partial \nu} \mid_{\partial\Omega} = 0, \quad \frac{\partial v}{\partial \nu} \mid_{\partial\Omega} = 0.$$

The functions u, v are unknowns representing concentrations of chemical substances U, V. The parameter F denotes the rate at which the chemical substance U is being added during the chemical reaction, $F + k$ is the rate of $V \to P$ transformation and D_u, D_v are the diffusion constants. We denote right-hand sides in the system (7)-(8) by $F_1(u,v) = F(1-u) - uv^2$, $F_2(u,v) = -(F+k)v + uv^2$.

The system (7-8) does not possess the invariant region for realistic parameter values. However, the comparison techniques allow to obtain the L_∞ bounds for the solution as provided by the following statement.

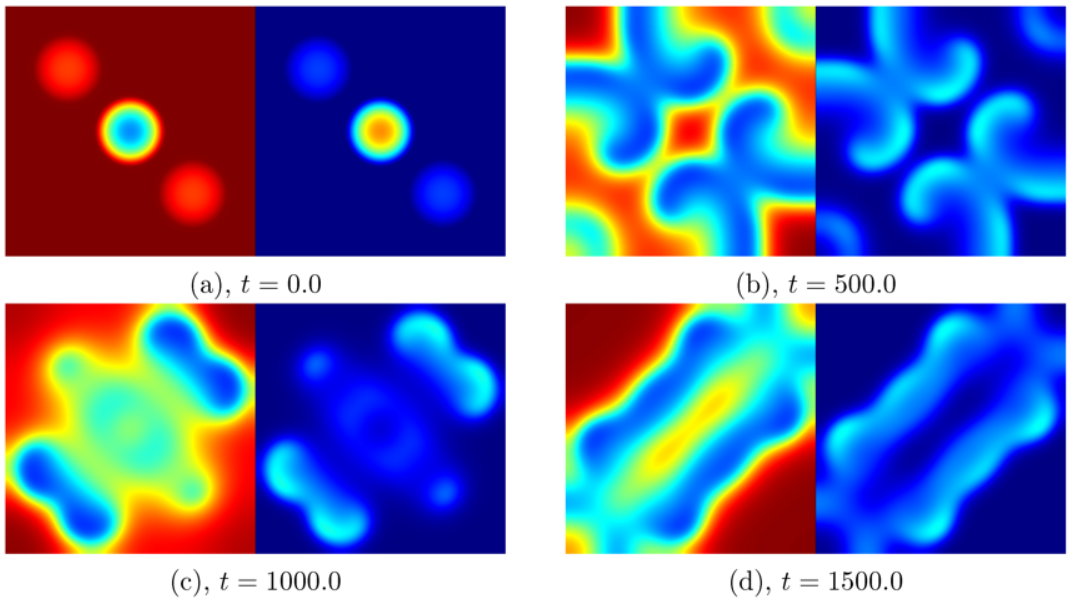

(a), $t = 0.0$ (b), $t = 500.0$

(c), $t = 1000.0$ (d), $t = 1500.0$

Figure 1: Chaotic behavior of the solution components u (left) and v (right) is schematically shown in color scale. The model parameters are $a = 2 \cdot 10^{-5}$, $b = 1 \cdot 10^{-5}$, $F = 0.02$, $k = 0.05$, $\Omega = (0, 0.5) \times (0, 0.5)$.

Theorem 3. *Consider the system (7-8). Let $T > 0$ be arbitrary fixed, and the initial condition $u_{ini}, v_{ini} \in \mathrm{L}_\infty(\Omega)$ satisfies*

$$0 \le u_{ini}(x) \le 1, \quad 0 \le v_{ini}(x) \le M \quad \forall x \in \Omega,$$

where $0 < M < F + k$. Then the solution u, v of the problem (7-8) satisfies the inequalities

$$0 \le u(t, x) \le 1, \quad 0 \le v(t, x) \le M \quad \forall (t, x) \in (0, T) \times \Omega.$$

Furthermore, under these assumptions, the nonlinear Galerkin method converges for system (7-8).

Proof follows from [25] and [40].
Example of the complex spatio-temporal dynamics obtained in [39] is shown in Figure 1.

3.1.2 Scott-Wang-Showalter model in combustion

The combustion is a chemical and physical phenomenon that is difficult to accurately describe by a mathematical model. However, we can discuss an example of combustion of pre-mixed hydrocarbon gases described by a reaction-diffusion model.

In this case, the target patterns were experimentally observed. These patterns were created by the combustion of simple hydrocarbon gases and other elements; e.g., butane or octane mixed with oxygen and helium. A formation and a temporal evolution of the above mentioned patterns can be modelled by the Salnikov scheme [54]:

$$\begin{aligned} P &\longrightarrow A \\ A &\longrightarrow B + heat \ , \end{aligned}$$

where the rate of the first reaction is $k_1 p$ and the rate of the second reaction is $k_2 a$, k_1, k_2 are the rate constants and p, a denote the concentrations of P, A species. The k_2 factor depends on temperature T and this dependence is of the Arrhenius type. According to [54], we can describe the concentration of the intermediate species A and the temperature T by a system of partial differential equations

$$\begin{aligned}\frac{\partial a}{\partial \tau} &= k_1 p_0 - k_2(T)a + D_A \Delta a,\\ \frac{\partial T}{\partial \tau} &= \frac{Q}{C_p \sigma} k_2(T) a - \frac{T - T_a}{t_N} + D_T \Delta T,\end{aligned}$$

where p_0 is the concentration of the initial species P, T is the temperature, D_A is the mass diffusivity of the species A, D_T is the thermal diffusivity, $C_p\sigma$ is the volumetric heat capacity (assumed to remain constant), t_N is the heat transfer timescale, T_a is the ambient temperature.

These equations can be transformed into the dimensionless form as follows

$$\begin{aligned}\frac{\partial \alpha}{\partial t} &= \mu - \alpha f(\Theta) + \Delta \alpha,\\ \frac{\partial \Theta}{\partial t} &= \frac{1}{\kappa}\left(\alpha f(\Theta) - \Theta\right) + Le \Delta \Theta,\end{aligned} \tag{9}$$

which is known as the Scott-Wang-Showalter model. Here, Le constant denotes the Lewis number ($Le = \frac{D_T}{D_A}$). The function f is defined as

$$f(\Theta) = \exp\left(\frac{\Theta}{1 + \varepsilon \Theta}\right).$$

Furthermore,

$$\Theta = \frac{E(T - T_a)}{R T_a^2}, \quad \alpha = \frac{a}{c_{ref}}, \quad t = \frac{\tau}{t_{chem}}, \quad x = \frac{\tilde{x}}{l_{ref}}, \quad y = \frac{\tilde{y}}{l_{ref}}, \tag{10}$$

where

$$t_{chem} = \frac{1}{k_{2,a}}, \quad c_{ref} = \frac{C_p \rho}{Q} \frac{R T_a^2}{E} \frac{t_{chem}}{t_N}, \quad l_{ref} = (D_A t_{chem})^{\frac{1}{2}}.$$

Finally, we rewrite the Arrhenius equation $k_2(T) = A \exp\left(-\frac{E}{RT}\right)$ as $k_2(T) = k_{2,a} f(\Theta)$, where $k_{2,a}$ is a value of function $k_2(T)$ in ambient temperature of T_a.

If system (9) is studied in $\Omega \subset \mathbb{R}^2$ over the period $(0, T)$ then we add the initial condition:

$$\alpha|_{t=0} = \alpha_{ini}, \qquad \Theta|_{t=0} = \Theta_{ini}.$$

and the boundary conditions of the Dirichlet type as follows:

$$\alpha|_{\partial\Omega} = \frac{\mu}{\mathrm{e}^{\left(\frac{\mu}{1+\varepsilon\mu}\right)}}, \qquad \Theta|_{\partial\Omega} = \mu.$$

or of the Neumann type as follows:

$$\left.\frac{\partial \alpha}{\partial n}\right|_{\partial\Omega} = 0, \qquad \left.\frac{\partial \Theta}{\partial n}\right|_{\partial\Omega} = 0,$$

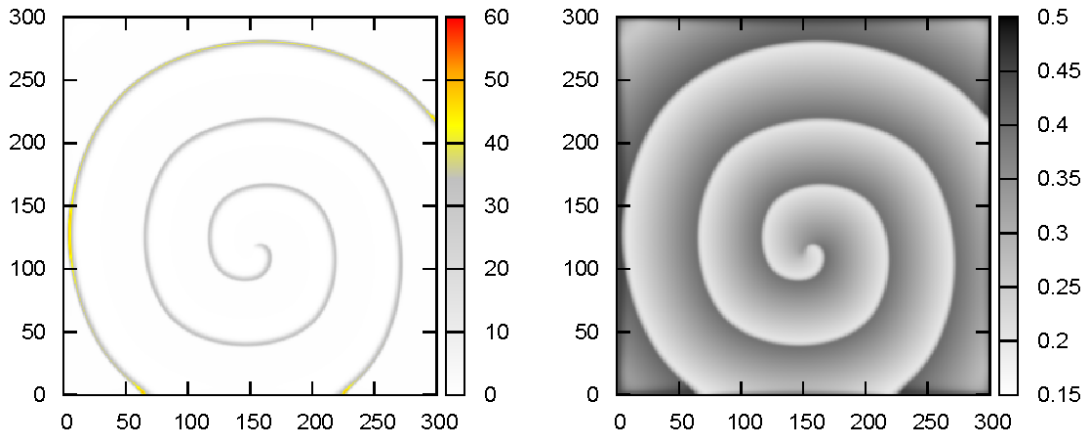

Figure 2: Temperature field (left) and concentration field (right) in color scale at time $t = 0.9$ shows a spiral-wave pattern observed in the experiment as well. The spatial scale indicates the grid size 300×300 on the domain $\Omega = (0, 30) \times (0, 30)$.

where $\vec{n}$ is outer normal vector to the boundary of the domain Ω.

Theorem 4. *Consider system (9). Then for the parameter values $\mu = 2.5$, $\epsilon = 0.18$, $\kappa = 0.0005$, it possesses the invariant region*

$$0.01 \leq \alpha \leq 2.5, \quad 0.01 \leq \Theta \leq 616.$$

Proof follows from [61].

Consequently, the framework of Section 3.1 is applicable to system (9). Figure 2 shows a spiral-wave pattern developed for $\mu = 2.6$, $Le = 1.5$, $\epsilon = 0.18$, $\kappa = 0.0005$ on the domain $\Omega = (0, 30) \times (0, 30)$ as presented in [35].

3.2 Moving interfaces in material science

Complex diffusion phenomena accompany physical processes taking place in crystalline materials - phase transitions, thin surface layer evolution or dynamics of material defects. These phenomena are discussed below.

3.2.1 Microstructure in solidification

The solidification of a pure material belongs to the class of first-order phase transitions where the energy of self-organization is released during the process. The Stefan problem for melting or freezing is obtained by evaluating the heat balance of the system. Formation of microstructure in the system is the result of changes in an other kind of energy, linked to the structural organization (free energy or entropy). Heat and free energy interact during the transient solidification process and can lead to the development of unstable complex shapes in the solid subdomain (e.g., cells, dendrites). A detailed analysis of the phase transition with more kinds of energy has been performed in [33, 34, 5].

Let $\Omega \subset \mathbb{R}^2$ be a bounded domain where the phase transition occurs, $\Omega_l(t)$, $\Omega_s(t)$ liquid and solid subdomain, respectively separated by the moving interface Γ (see Figure 3), $\langle 0, T\rangle$ a time interval, $u : \langle 0, T\rangle \times \bar{\Omega} \to \mathbb{R}$ the temperature field.

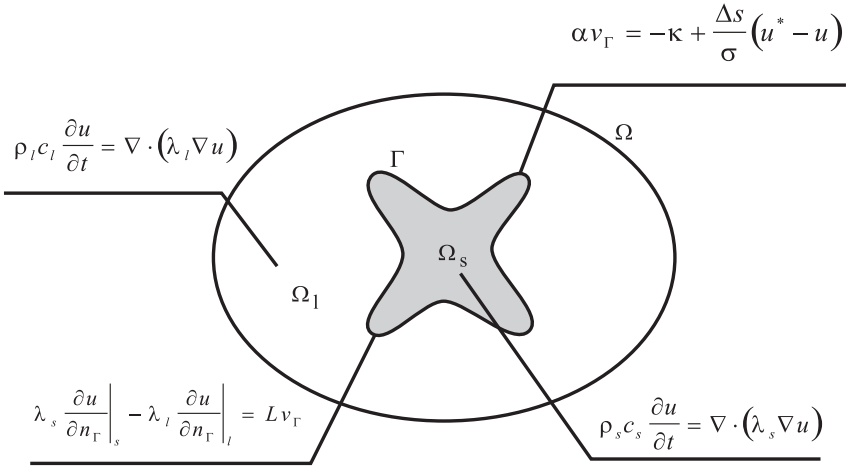

Figure 3: Domain Ω divided into the growing solid and vanishing liquid.

The process of phase change at small scale is according to [33] and [5] described by the Stefan problem with surface tension in the following form:

$$\rho c \frac{\partial u}{\partial t} = \nabla(\lambda \nabla u) \qquad \text{in } \Omega_s \text{ and } \Omega_l \quad , \tag{11}$$

$$u \mid_{\partial\Omega} = u_{\partial\Omega} \quad , \tag{12}$$

$$u \mid_{t=0} = u_0 \quad , \tag{13}$$

$$\lambda \frac{\partial u}{\partial n} \mid_s - \lambda \frac{\partial u}{\partial n} \mid_l = L v_\Gamma \quad , \tag{14}$$

$$u - u^* = -\frac{\sigma}{\Delta s}\kappa - \alpha \frac{\sigma}{\Delta s} v_\Gamma \quad , \tag{15}$$

$$\Omega_s(t) \mid_{t=0} = \Omega_{so} \quad . \tag{16}$$

where ρ, c, λ, L are the density, volumetric heat capacity, heat conductivity and latent heat, respectively. The interface Γ has the mean curvature denoted by κ, the normal velocity v_Γ (in the direction of the outer normal $\mathbf{n}_\Gamma$ to Ω_s), the surface tension σ and the difference in entropy densities Δs.

The discontinuity of heat flux on $\Gamma(t)$ is described by the Stefan condition (14), the formula (15) is the Gibbs-Thompson relation on $\Gamma(t)$ and α is the coefficient of attachment kinetics. The Dirichlet boundary condition (12) is chosen for simplicity. The conditions (13) and (16) are the initial conditions for temperature, and spatial distribution of the solid and liquid phase.

Among various approaches to the mathematical treatment of the problem (e.g. see [63]), the diffuse-interface model yields a well controlled smooth approximation of the characteristic function of phase as a part of the solution (see [5]). The model equations consist of the heat equation with nearly singular heat source coupled to a semilinear or quasilinear parabolic equation for the order parameter known as the Allen-Cahn equation or equation of phase. The equations in various setting were studied in, e.g. [16, 6] and in references therein. The anisotropy has been incorporated in [4, 7]. A recent study [26] lists current achievements in this domain.

The anisotropic form of the phase-field model of microstructure formation reads as

$$\begin{aligned} \frac{\partial u}{\partial t} &= \nabla^2 u + L\chi'(p)\frac{\partial p}{\partial t}, \\ \xi \frac{\partial p}{\partial t} &= \xi \nabla \cdot T^0(\nabla p) + \frac{1}{\xi} f_0(p) + F(u)\xi \Phi^0(\nabla p), \end{aligned} \tag{17}$$

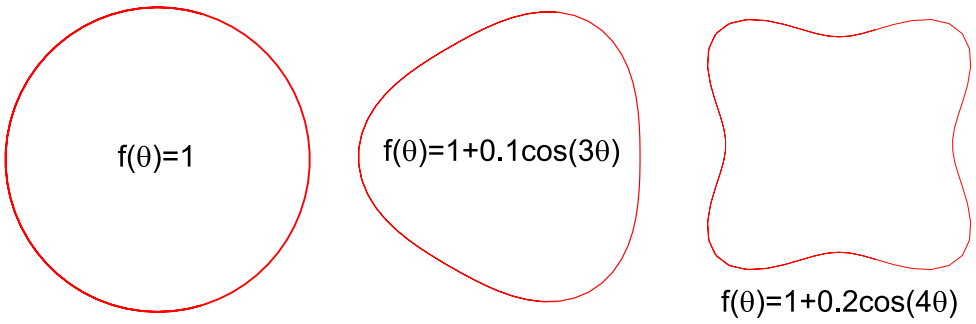

Figure 4: The Frank diagram of anisotropy.

with the initial conditions

$$u|_{t=0} = u_0 \ , \quad p|_{t=0} = p_0 \quad ,$$

and with the boundary conditions of Dirichlet type

$$u|_{\partial\Omega} = 0 \ , \quad p|_{\partial\Omega} = 0,$$

for simplicity. Here, $\xi > 0$ is the "small" parameter (thickness of the interface), and f_0 the derivative of double-well potential. The coupling function $F(u)$ is bounded and continuous, or even Lipschitz-continuous. The anisotropy is included using the monotone operator T^0 converting the gradient (see below). We consider $f_0(p) = ap(1-p)(p-\frac{1}{2})$ with $a > 0$. The enthalpy is given by $\mathcal{H}(u) = u - L\chi(p)$, where the coupling function χ is monotone with bounded, Lipschitz-continuous derivative: $\chi(0) = 0$, $\chi(0.5) = 0.5$, $\chi(1) = 1$, $supp(\chi') \subset \langle 0, 1\rangle$. For the sake of simplicity, Ω is rectangle. Obviously, the extension to higher dimensions, and to other boundary conditions is possible. The forcing term $F(u)\xi\Phi^0(\nabla p)$ has the origin described in [3].

The anisotropy is incorporated into the phase-field model according to the approach developed by the author in [4] and [7], which also is influenced by the literature cited therein. Main idea is in replacing isotropic Euclidean norm in $\mathbb{R}^2$ by another norm exhibiting the desired anisotropy, and in replacing derivatives in a corresponding way.

For this purpose, we introduce a nonnegative function $\Phi^0 : \mathbb{R}^2 \to \mathbb{R}_0^+$ which is smooth, strictly convex, $\mathcal{C}^2(\mathbb{R}^n \setminus \{\Theta\})$ and satisfies:

$$\Phi^0(t\eta) = |t|\Phi^0(\eta), \quad t \in \mathbb{R}, \eta \in \mathbb{R}^2, \tag{18}$$

$$\lambda|\eta| \leq \Phi^0(\eta) \leq \Lambda|\eta|, \tag{19}$$

where $\lambda, \Lambda > 0$. The function satisfies the following relation

$$\Phi^0(\eta) = \Phi^0_\eta(\eta) \cdot \eta, \quad \eta \in \mathbb{R}^2,$$

where the index η denotes derivative of Φ^0 (i.e., $\Phi^0_\eta = (\partial_{\eta_1}\Phi^0, \partial_{\eta_2}\Phi^0)$). We define the map $T^0 : \mathbb{R}^2 \to \mathbb{R}^2$ as

$$\begin{aligned} T^0(\eta) &:= \Phi^0(\eta)\Phi^0_\eta(\eta) \text{ for } \eta \neq 0, \\ T^0(0) &:= 0. \end{aligned}$$

The Φ^0-normal vector and velocity of a level set

$$\Gamma(t) = \{x \in \mathbb{R}^2 \mid P(t,x) = const.\},$$

given by a suitable field P depending on time and space are

$$\mathbf{n}_{\Gamma,\Phi} = -\frac{T^0(\nabla P)}{\Phi^0(\nabla P)}, \quad v_{\Gamma,\Phi} = \frac{\partial_t P}{\Phi^0(\nabla P)}.$$

The anisotropic curvature is given by the formula

$$\kappa_{\Gamma,\Phi} = div(\mathbf{n}_{\Gamma,\Phi}).$$

In [7, 9], the law

$$v_{\Gamma,\Phi} = -\kappa_{\Gamma,\Phi} + F,$$

has been studied by the phase-field method, in particular by the Allen-Cahn equation as in (17).

Example. In case of $\mathbb{R}^2$, we may use the polar coordinates of a vector $\eta \in \mathbb{R}^2$ denoted by ϱ and θ to define

$$\Phi^0(\eta) = \varrho f(\theta),$$

for a suitable 2π-periodic function f (we choose $f(\theta) = 1 + A\cos(m(\theta - \theta_0))$ where A is the anisotropy strength and $m \in \mathbb{N}_0$ the anisotropy type). Φ^0 therefore belongs to $\mathcal{C}^1(\mathbb{R}^2)$ and $\mathcal{C}^2(\mathbb{R}^2 \setminus \{0\})$ provided Ψ belongs to $\mathcal{C}^2(\langle 0, 2\pi\rangle_{per})$. Figure 4 depicts the Frank diagram for an example of f - see [34] for definitions.

The analysis of problem (17) is related to numerical studies obtained by the model both for the case of curve dynamics in the plane (see [7]), and for the case of microstructure growth in solidification (see [4, 9]).

The system (17) has been analysed in [5, 4] from where the following statement follows:

Theorem 5. *Assume that problem (17) is solved in a bounded domain $\Omega \subset \mathbb{R}^2$ with C^2 boundary and homogeneous Dirichlet boundary conditions, T^0 monotone, and F bounded continuous, χ the function with properties $\chi(0) = 0, \chi(1) = 1, \chi(0.5) = 0.5$, χ' bounded and Lipschitz continuous with support $\langle 0, 1\rangle$. Let $\xi > 0$ be fixed and $u_{ini}, p_{ini} \in \mathrm{H}_0^1(\Omega)$. Then there exists the weak solution satisfying, in terms of $\mathcal{D}'(0,T)$, the equalities*

$$\begin{aligned} \frac{d}{dt}(u - L\chi(p), v) + (\nabla u, \nabla v) &= 0 \quad , \\ \alpha\xi^2 \frac{d}{dt}(p, q) + \xi^2(T^0(\nabla p), \nabla q) &= (f_0(p), q) + \xi^2(F(u)\Phi^0(\nabla p), q) \quad , \\ u|_{t=0} = u_{ini}, \qquad & p|_{t=0} = p_{ini}. \end{aligned}$$

for each $v, q \in \mathrm{H}_0^1(\Omega)$, and satisfying

$$u, p \in \mathrm{L}_\infty(0, T; \mathrm{H}_0^1(\Omega)),\ \frac{\partial u}{\partial t}, \frac{\partial p}{\partial t} \in \mathrm{L}_2(0, T; \mathrm{L}_2(\Omega)) \quad .$$

If F is Lipschitz continuous, $\chi' \equiv 1$ and T^0 is strictly monotone, the weak solution is unique.

Proof explores the properties of (17) and is based on the compactness and monotonicity method.

The matched asymptotics as used e.g. in [5] gives the recovery of the Stefan condition and the Gibbs-Thomson law at the phase interface.

In this procedure, the solution and other quantities of (17) are formally expanded into the series in powers of ξ far from Γ:

$$\begin{aligned} u(t,x;\xi) &= u_0(t,x) + u_1(t,x)\xi + u_2(t,x)\xi^2 + \mathcal{O}(\xi^3), \\ p(t,x;\xi) &= p_0(t,x) + p_1(t,x)\xi + p_2(t,x)\xi^2 + \mathcal{O}(\xi^3), \end{aligned}$$

and near Γ with the change to radial-tangential coordinates r, s and stretching $r = \xi z$

$$\begin{aligned} \bar{u}(z,s,t;\xi) &= \bar{u}_0(z,s,t) + \bar{u}_1(z,s,t)\xi + \bar{u}_2(z,s,t)\xi^2 + \mathcal{O}(\xi^3), \\ \bar{p}(z,s,t;\xi) &= \bar{p}_0(z,s,t) + \bar{p}_1(z,s,t)\xi + \bar{p}_2(z,s,t)\xi^2 + \mathcal{O}(\xi^3). \end{aligned}$$

Defining $\Gamma_0 \equiv \bar{p}_0 = \frac{1}{2}$ and exploring identities at corresponding powers of ξ, the following statement is obtained:

Theorem 6. *On the manifold Γ_0, the Stefan condition for the absolute terms in the outer expansion of temperature holds:*

$$|\nabla r|^2 \left(\left.\frac{\partial u_0}{\partial r}\right|_s - \left.\frac{\partial u_0}{\partial r}\right|_l \right) = L v_{\Gamma,\Phi,0},$$

and the Gibbs-Thomson law for the absolute term in the inner expansion of the phase function holds:

$$\int_{\mathbb{R}} \left(-\kappa_{\Gamma,\Phi,0} \frac{\partial \bar{p}_0}{\partial z} - F(\bar{u}_0) \left| \frac{\partial \bar{p}_0}{\partial z} \right| - \frac{\partial \bar{p}_0}{\partial z} v_{\Gamma,\Phi,0} \right) \frac{\partial \bar{p}_0}{\partial z} dz = 0.$$

We solve equations (17) numerically by means of the tools used in [5, 9]. Using the notation introduced in Section 2.2, we propose a semi-discrete scheme for the problem (17) based on spatial discretization by finite differences as follows

$$\dot{u}^h = \Delta_h u^h + L\chi'(p^h)\dot{p}^h, \tag{20}$$
$$u^h \mid_{\gamma_{\mathbf{h}}} = 0, \quad u^h(0) = \mathcal{P}_h u_0,$$
$$\xi^2 \dot{p}^h = \xi^2 \nabla_h \cdot T^0(\bar{\nabla}_h p^h) + f_0(p^h) + \xi^2 \Phi^0(\bar{\nabla}_h p^h) F(u^h) \text{ on } \omega_{\mathbf{h}}, \tag{21}$$
$$p^h \mid_{\gamma_{\mathbf{h}}} = 0, \quad p^h(0) = \mathcal{P}_h p_0,$$

where the solution is the map $u^h, p^h : \langle 0, T\rangle \to \mathcal{H}_h$, $\mathcal{P}_h$ restricts the initial condition u_0 and u_0 on the grid $\bar{\omega}_h$. As in [5], [7] and related work, the semi-discrete scheme is solved by the Merson variant of the 4-th order Runge-Kutta method. We mention, that the scheme (20-21) is convergent.

Theorem 7. *If $u_{ini}, p_{ini} \in \mathrm{H}^2(\Omega) \cap \mathrm{H}_0^1(\Omega)$, then the solution of the semi-discrete scheme (20-21) for the method of lines converges in $\mathrm{L}_2(0,T;\mathrm{L}_2(\Omega))$ to the weak solution of (17).*

Figure 5 shows an example of numerically solved pattern formation in solidification as described in [26].

3.2.2 Surface diffusion

Within the context of solid state physics and material science, the evolution law of surface diffusion can be investigated. The mentioned law is described, e.g. in the results of Mullins

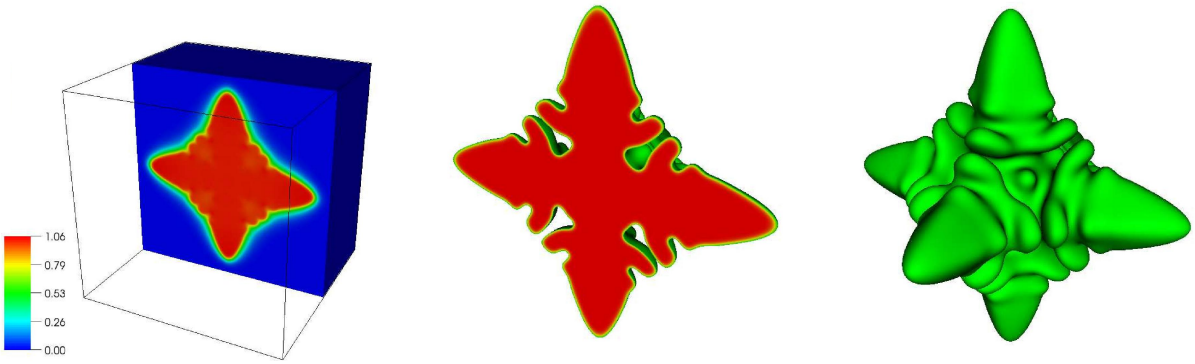

Figure 5: Three-dimensional dendritic growth with four-folded anisotropy and parameters $u^* = 1.0$, $L = 2.0$, $\beta = 300$, $a = 2.0$, $\alpha = 3$, $L_1 = L_2 = L_3 = 4.0$, initial radius $= 0.05$, $N_1 = N_2 = 400$, $\xi = 0.011$. Left - the temperature profile.

[46], [47] as a mechanism of surface formation under the action of chemical potential. Further interesting application is in the microcrack formation as given in [1]. The law reads as

$$V = \Delta_\Gamma(H + F) \text{ on } \Gamma, \tag{22}$$

for two-dimensional surfaces Γ embedded in the Euclidean three-dimensional space $\mathbb{R}^3$, which can be represented by graphs. Here, $\Gamma(t)$ is the evolving surface in $\mathbb{R}^3$, $\mathbf{n}_\Gamma$ the normal vector to Γ, V the normal velocity of Γ, Δ_Γ the Laplace-Beltrami operator with respect to Γ, H the mean curvature of Γ (the sum of principal curvatures), F the forcing term.

The problem has been studied, e.g. in [8] and in references therein. The purpose of the research is to provide a suitable tool for the study of surface phenomena accompanying special surface treatment or behavior of surfaces under the influence of external forces. The general field of application of the developed model can be in the body-shape dynamics as a result of surface processes, surface destruction as a result of external stress and vibration, computer data processing.

We also mention a certain diversity in the physical and mathematical terminology, as indicated by [36]. Mathematical understanding of this phenomenon is related to the shape changes due to the redistribution of the matter below the surface, whereas physical investigation considers the surface atomic redistribution processes.

Graph formulation. Our scope is given by the fact that we intend to study the evolution of surfaces as graphs of real functions of two variables. More precisely, we assume that there is a function $\Phi : \mathbb{R}^{1+2} \to \mathbb{R}$ such that

$$\Gamma(t) = \{[x, y] \in \mathbb{R}^3 \mid y = \Phi(t, x), x \in \Omega \subset \mathbb{R}^2\}.$$

For simplicity, we assume that $\Omega = (0, L_1) \times (0, L_2) \subset \mathbb{R}^2$ is an open rectangle, we also denote by $\partial\Omega$ its boundary, by $\mathbf{n}_{\partial\Omega}$ its outer normal and by ∂_n the normal derivative with respect to $\mathbf{n}_{\partial\Omega}$. Consequently, law (22) can be reformulated into the evolution equations

$$\frac{\partial \Phi}{\partial t} = \nabla \cdot (Q(\nabla\Phi)(\nabla(H + F) - (\nabla(H + F) \cdot \mathbf{N})\mathbf{N})), \tag{23}$$

$$H = -\nabla \cdot \left(\frac{\nabla\Phi}{Q(\nabla\Phi)} \right). \tag{24}$$

which are viewed as the fourth-order PDE with respect to Φ. For simplicity, it is endowed with the Dirichlet boundary conditions:

$$\Phi|_{\partial\Omega} = 0, \quad H|_{\partial\Omega} = 0, \tag{25}$$

or alternatively, with the Neumann boundary conditions:

$$\left.\frac{\partial\Phi}{\partial n}\right|_{\partial\Omega} = 0, \quad \left.\frac{\partial H}{\partial n}\right|_{\partial\Omega} = 0, \tag{26}$$

and by the initial condition

$$\Phi|_{t=0} \;=\; \Phi_{ini}. \tag{27}$$

The boundary conditions (25)/(26) can be generalized. In [8] the following basic solution properties are shown:

Theorem 8. *Let Φ, H be a solution to the initial-boundary value problem (23-24) with $F = 0$. Then the following properties hold:*

$$\frac{d}{dt}\int_\Omega \Phi dx = 0,$$

provided the boundary conditions (26) are imposed, and

$$\frac{d}{dt}\int_\Omega Q(\nabla\Phi)dx + \int_\Omega \left(|\nabla H|^2 - |\nabla H\cdot\mathbf{N}|^2\right) Q(\nabla\Phi)dx = 0,$$

provided the boundary conditions either (25), or (26) are imposed.

For the purpose of **numerical solution** of the law (23-24), we derive a numerical scheme based on the method of lines together with the finite-difference discretization of spatial derivatives. We use the notation introduced in Section 2.2. We also use a projection operator $\mathcal{P}_h : \mathcal{C}(\Omega) \to \mathbb{R}^{N_1+1,N_2+1}$ defined as $\mathcal{P}_h g = g|_{\bar\omega_h}$. The discretization of the Neumann boundary conditions is performed by means of the finite-difference approximation of normal derivatives. Then, we propose a semi-discrete scheme containing a time-dependent system of ODEs for the unknown functions $\Phi^h, H^h : (0,T)\times\bar\omega_h \to \mathbb{R}$

$$\frac{d\Phi^h}{dt} \;=\; \nabla_h\cdot\left(Q(\bar\nabla_h\Phi^h)(\bar\nabla_h(H^h+F) - (\bar\nabla_h(H^h+F)\cdot\mathbf{N}^h)\mathbf{N}^h\right), \tag{28}$$

$$H^h \;=\; -\nabla_h\cdot\left(\frac{\bar\nabla_h\Phi}{Q(\bar\nabla_h\Phi^h)}\right), \quad \mathbf{N}^h = -\frac{\bar\nabla_h\Phi^h}{Q(\bar\nabla_h\Phi^h)}. \tag{29}$$

According to (25)/(26), we consider two pairs of boundary conditions, alternatively:

$$\Phi^h\big|_{\gamma_h} = 0, \quad H^h\big|_{\gamma_h} = 0, \tag{30}$$

or

$$\Phi^h_{\bar n}\big|_{\gamma_h} = 0, \quad H^h_{\bar n}\big|_{\gamma_h} = 0. \tag{31}$$

The initial condition is written as follows

$$\Phi^h\big|_{t=0} = \mathcal{P}_h\Phi_{ini}.$$

The scheme (28-29) is a system of first-order differential equations in the initial-value problem. We resolve it by means of the Runge-Kutta method with the step adaptivity (Merson variant) as described in [7]. The scheme (28-29) exhibits similar features to Theorem 8 as shown in [8]. Figure 6 shows an example of singular behaviour when a perturbation leads to the pinch-off in longterm.

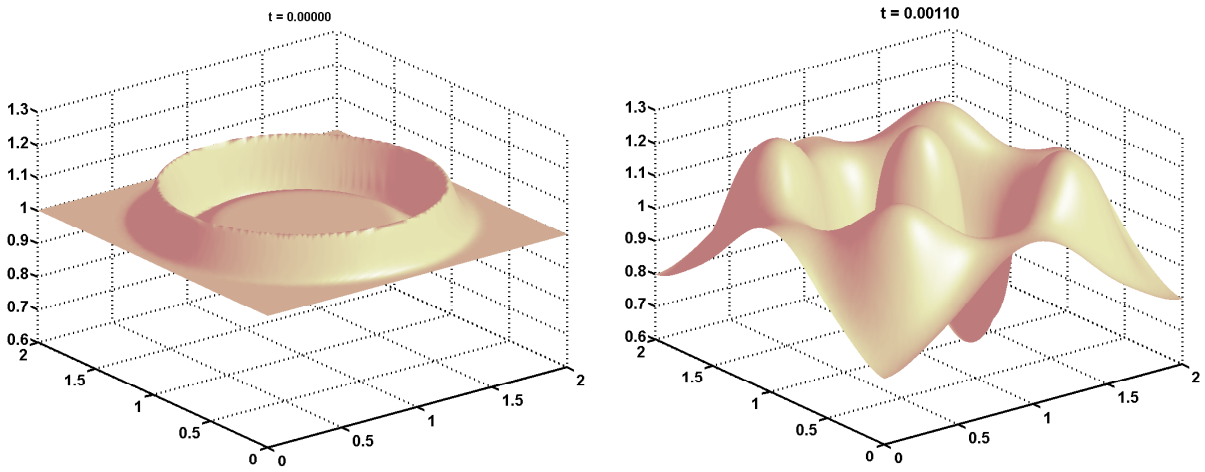

Figure 6: Example of solution of (23) - the shape which develops in time ($F = -\frac{100}{\Phi}$).

3.2.3 Dislocation dynamics

Discrete dislocation dynamics is devoted to the study of interactions between one or more dislocation curves and several other defects such as dipolar loops. The mentioned objects are located in a bounded 3D domain.

At low-temperature, glide dislocations can be represented as smooth planar curves. As described in earlier results such as [24, 45, 44] and in references therein, motion of the dislocation curve Γ can be described by the evolution law

$$Bv_\Gamma = -T\kappa_\Gamma + F, \tag{32}$$

relating its normal velocity v_Γ to the curvature κ_Γ and sum F of forces acting on Γ in the normal direction. Here, B denotes the drag coefficient and T stands for the line tension. Due to the term with the surface tension, law (32) belongs to the category of diffusive processes. Among other properties, it has the same form as the Gibbs-Thomson law in the model of phase transitions described in Section 3.2.1.

The parametric description of (32) is suitable for dislocation dynamics as such material defects are represented by open curves (see [44, 12]). Self-intersections as well as other topological changes can be incorporated into this approach in an algorithmic way.

For this purpose, we introduce notation for quantities related to this representation. A planar curve $\Gamma(t)$ evolving during the time interval $\langle 0, T\rangle$ can be described parametrically by a smooth vector mapping $\vec{X} : \langle 0, T\rangle \times \langle 0, 1\rangle \to \mathbb{R}^2$ depending on time and on parameter u from a fixed bounded interval $\langle 0, 1\rangle$. Then, the curve is expressed as

$$\Gamma(t) = \{\vec{X}(t, u) = [X^1(t, u), X^2(t, u)] \mid u \in \langle 0, 1\rangle\}.$$

The unit tangential vector to the curve $\vec{T}$ is defined as $\vec{T} = \partial_u\vec{X}/|\partial_u\vec{X}|$. The unit normal vector to the curve $\vec{N}$ is perpendicular to the tangential vector in selected direction and

is denoted as $\vec{N} = \partial_u \vec{X}^{\perp}/|\partial_u \vec{X}|$. The Frenet formulae (see e.g. [64, 12]) and expressions for other relevant quantities lead to the reformulation of (32) into the equation for parametrization $\vec{X} = \vec{X}(t,u)$ in the form

$$\partial_t \vec{X} = T\frac{\partial^2_{uu}\vec{X}}{|\partial_u \vec{X}|^2} + F\frac{\partial_u \vec{X}^{\perp}}{|\partial_u \vec{X}|}, \tag{33}$$

where law (32) can be recovered by multiplying the vectorial equation (33) by the vector $\vec{N}$.

This equation is accompanied either by the periodic boundary conditions

$$\vec{X}(t,0) = \vec{X}(t,1),$$

for closed dislocation curves (e.g. appearing in the Frank-Read source), or with fixed ends

$$\vec{X}(t,0) = \vec{X}_{\text{fixed},0},\ \vec{X}(t,1) = \vec{X}_{\text{fixed},1},$$

for open dislocation curves. The initial condition for the curve position is prescribed as

$$\vec{X}(0,u) = \vec{X}_{\text{ini}}(u).$$

The dislocation curves interact dynamically with other material defects such as dipolar loops through the elastic force field. The xz-plane represents the dislocation glide plane. The dipolar loops are considered in their stable configurations - having long rectangular fixed shapes (see [44] and references therein).

Therefore their motion can be fully described by motion of their barycenters, at the given level of approximation. They are assumed to have longer edges parallel with the z-axis whereas their shorter edges are parallel with either $[1,1,0]$ or $[1,-1,0]$ vectors. This means that a dipolar loop can move along the x-axis only, keeping the y- and z-coordinates constant. The Burgers vector is set as $\vec{b} = [b,0,0]$.

As indicated above, each dipolar loop is assumed to have a rectangular shape and to have one of the two stable configurations in the atomic lattice depending of the defect type - vacancy (i.e. V_1, V_2) and interstitial (i.e. I_1, I_2) configurations - see [44]. We also assume that dipolar loops have the same size which is described by the average half-width h, the average half-length l, and the average perimeter $P = 2\left(2h\sqrt{2} + 2l\right)$ as can be seen in [44]. The position of a dipolar loop $\Lambda_j,\ j = 1,\dots,N$ is given by the coordinates $\left[x^{(j)}, y^{(j)}, z^{(j)}\right]$ of its barycenter. According to the previous assumptions, $y^{(j)} = const. \neq 0$ and $z^{(j)} = const.$, whereas $x^{(j)} = x^{(j)}(t)$ is given by the motion law

$$\frac{\mathrm{d}x^{(j)}}{\mathrm{d}t} = \frac{1}{BP}F^{(j)}_{x,\text{total}}\left(\Gamma, x^{(1)},\dots,x^{(N)}\right), \tag{34}$$

where the term $F^{(j)}_{x,\text{total}}$ is given by the force interaction with other dipolar loops and with the dislocation curve $\Gamma(t)$ described by the parametrization $\vec{X}$. This interaction is projected to the only possible direction of the loop motion - to the direction of the x-axis.

The interaction dynamics of dislocation curves $\Gamma_1,\dots,\Gamma_K$ parametrized by $\vec{X}^{(1)},\dots,\vec{X}^{(K)}$ and dipolar loops $\Lambda_1,\dots,\Lambda_N$ is therefore described by the following set of equations en-

dowed with the boundary and initial conditions

$$\partial_t \vec{X^{(l)}} = T\frac{\partial^2_{uu}\vec{X^{(l)}}}{|\partial_u \vec{X^{(l)}}|^2} + F(t, \vec{X^{(1)}}, \ldots, \vec{X^{(M)}}, \Lambda_1, \ldots, \Lambda_N)\frac{\partial_u \vec{X^{(l)}}^{\perp}}{|\partial_u \vec{X^{(l)}}|}, \quad (35)$$

$$\vec{X^{(l)}}(t,0) = \vec{X^{(l)}}_{\text{fixed},0}, \quad \vec{X^{(l)}}(t,1) = \vec{X^{(l)}}_{\text{fixed},1},\ l = 1, \ldots, K, \quad (36)$$

$$\vec{X^{(l)}}(0,u) = \vec{X^{(l)}}_{\text{ini}}(u),\ l = 1, \ldots, K \quad (37)$$

$$\frac{\mathrm{d}x^{(j)}}{\mathrm{d}t} = \frac{1}{BP}F^{(j)}_{x,\text{total}}\left(\vec{X^{(1)}}, \ldots, \vec{X^{(K)}}, x^{(1)}, \ldots, x^{(N)}\right), \quad (38)$$

$$x^{(j)}(0) = x^{(j)}_{\text{ini}},\ j = 1, \ldots, N. \quad (39)$$

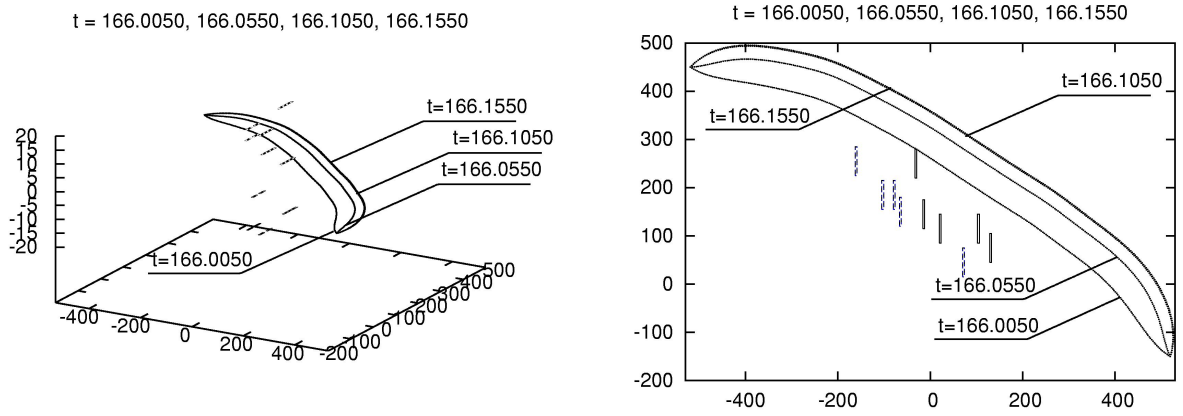

Figure 7: 10 dipolar loops of V1 and V2 type clustering together. The graph on the left shows the spatial positions of interacting dislocation and dipolar loops, the graph on the right shows the projection of positions onto the glide plane.

The equations are solved by means of a numerical scheme based on discretization of the model equations in space by the flowing finite-volume method (see [44] and Figure 8) and subsequently, on discretization of the model equations in time by the higher-order Runge-Kutta scheme.

For $M = 1$, the dislocation curve Γ is approximated by a piece-wise linear curve with vertices - nodes $\vec{X}_i(t), i = 0, ..., M_v$ in the glide plane. The end-points $\vec{X}_0$ and $\vec{X}_{M_v}$ are prescribed by the boundary conditions (36)

$$\vec{X}_0 = \vec{X}_{\text{fixed},0},\ \vec{X}_{M_v} = \vec{X}_{\text{fixed},L},$$

and do not depend on time. The following system of ordinary differential equations (ODE's) is obtained (compare with [12])

$$B\frac{\mathrm{d}\vec{X}_i}{\mathrm{d}t} = T\frac{2}{d_i + d_{i+1}}\left(\frac{\vec{X}_{i+1} - \vec{X}_i}{d_{i+1}} - \frac{\vec{X}_i - \vec{X}_{i-1}}{d_i}\right) + \frac{2}{d_i + d_{i+1}}F_i\frac{\vec{X}^{\perp}_{i+1} - \vec{X}^{\perp}_{i-1}}{2}, \quad (40)$$
$$i = 1, \ldots, M_v - 1\ .$$

with the initial conditions

$$\vec{X}_i(0) = \vec{X}_{\text{ini}}(s_i),\ i = 1, \ldots, M_v - 1.$$

Figure 7 shows an example of the dipolar-loop clustering by interaction with a moving dislocation as described in [43].

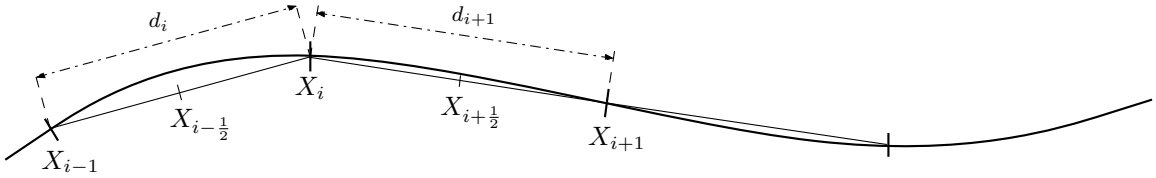

Figure 8: Piecewise linear approximation of the dislocation curve, flowing finite volumes and construction of dual volumes.

3.3 Diffusion in computer image processing

This work is motivated by the need of medical practice for evaluation of the dynamical images of the heart obtained by the magnetic resonance imaging (cardiac MRI). One of the important purposes of cardiac MRI examination is an estimation of parameters reflecting current clinical state of patients. A typical example could be an accurate measurement of heart ventricle volume during the heart contraction showing the contractive ability of myocardium. Within this framework, it is necessary to find the inner contour of the ventricle in the MR images. We attempt to adapt and modify a segmentation model based on numerical solution of a partial differential equation of the level set type. The iterative algorithm is controlled by the segmented image data in such a way that the edges of the objects can be found. The level set equation is solved by the semi-implicit complementary-volume numerical scheme [37].

A similar model used in image segmentation is based on the phase-field approach to the mean curvature flow. It is given by the Allen-Cahn equation (see [11]). In [18] the Allen-Cahn equation is used for segmentation of the left heart ventricle volume and the wall of the left heart ventricle. Recently, a priori information carried by the image data has been included into the segmentation models (see [51]).

In our case, the image is segmented by means of the curve $\Gamma(t) \subset \Omega$ in $\mathbb{R}^2$ propagating in the normal direction with speed V. The velocity V at a curve point $x \in \Gamma(t)$ is given by its (mean) curvature κ_Γ and external force as in Sections 3.2.1 and 3.2.3

$$V = -\kappa_\Gamma + F. \tag{41}$$

For the segmentation purposes, law (41) can be modified by incorporating the influence of the processed signal (or its gradient) into the curvature and the force terms. The motion law (41) can be treated by the level set method. In this case, $\Gamma(t)$ is represented as a level set

$$\Gamma(t) = \{x \in \Omega \,|\, u(t,x) = 0\}\,. \tag{42}$$

where $u : \langle 0, T\rangle \times \Omega \to \mathbb{R}$.

The evolution equation implicitly describing the motion of $\Gamma(t)$ given by (42) with velocity V in the outward normal direction is derived as follows. Using the convention introduced by the signed distance function, we can express the normal vector, the normal velocity and the mean curvature as

$$\vec{n} = \frac{\nabla u}{|\nabla u|}, \quad V = -\frac{\partial_t u}{|\nabla u|}, \quad \kappa_\Gamma = \nabla \cdot \vec{n} = \nabla \cdot \frac{\nabla u}{|\nabla u|}. \tag{43}$$

Substituting (43) to equation (41), we obtain the level set equation in the form

$$\partial_t u = |\nabla u| \nabla \cdot \frac{\nabla u}{|\nabla u|} - F|\nabla u|. \tag{44}$$

This equation has been extensively studied and applied (see [28], [50], [56]). This experience suggests a regularization useful both for theory and numerical computation in the form:

$$\partial_t u = |\nabla u|_\varepsilon \nabla \cdot \frac{\nabla u}{|\nabla u|_\varepsilon} - F|\nabla u|_\varepsilon,$$

where $|\nabla u|_\varepsilon = \sqrt{\varepsilon^2 + |\nabla u|^2}$.

Known features of the level set equation based mainly on the controlled motion of isolines of the solution naturally led to its use in the image processing (see [17], [42], [53], [56]).

In particular, the detection of image object edges (boundaries) is a one of tasks in image segmentation. Edges in the input image $I^0 : \Omega \to \{0, 1, 2 \ldots, I_{\max}\}$ (represented by the matrix $n_{x_1} \times n_{x_2}$, where $\Omega = (0, n_{x_1}/\max\{n_{x_1}, n_{x_2}\}) \times (0, n_{x_2}/\max\{n_{x_1}, n_{x_2}\})$ can be recognized by the magnitude of its spatial gradient. The level set equation operating in Ω can be modified as follows

$$\partial_t u = |\nabla u|_\varepsilon \nabla \cdot \left(g\left(\left|I^0 * \nabla G_\sigma\right|\right) \frac{\nabla u}{|\nabla u|_\varepsilon} \right) - g\left(\left|I^0 * \nabla G_\sigma\right|\right) |\nabla u|_\varepsilon F\,, \tag{45}$$

where $g : \mathbb{R}_0^+ \to \mathbb{R}^+$ is a non-increasing function for which $g(0) = 1$ and $g(s) \to 0$ for $s \to +\infty$. This function was first used by P. Perona and J. Malik ([52] in 1987) to modify the heat equation into a nonlinear diffusion equation which maintains edges in an image. Consequently, the function g is called the Perona-Malik function. We put $g(s) = 1/(1 + \lambda s^2)$ with $s \geq 0$. $G_\sigma \in \mathcal{C}^\infty(\mathbb{R}^2)$ is a smoothing kernel, e.g. the Gauss function with zero mean and variance σ^2

$$G_\sigma(x) = \frac{1}{\sqrt{2\pi\sigma^2}} e^{-\frac{|x|^2}{2\sigma^2}}, \tag{46}$$

which is used to pre-smoothing (denoising) of image gradients by convolution

$$(I^0 * \nabla G_\sigma)(x) = \int_{\mathbb{R}^2} \bar{I}^0(x - y) \nabla G_\sigma(y)\, \mathrm{d}y\,, \tag{47}$$

where $\bar{I}^0$ is the extension of I^0 to $\mathbb{R}^2$ by, e.g., mirroring, periodic prolongation or zero padding. Let us note that equation (45) can be rewritten into the advection-diffusion form

$$\partial_t u = \underbrace{g^0 |\nabla u|_\varepsilon \nabla \cdot \left(\frac{\nabla u}{|\nabla u|_\varepsilon} \right)}_{(D)} + \underbrace{\nabla g^0 \cdot \nabla u}_{(A)} - \underbrace{g^0 |\nabla u|_\varepsilon F}_{(F)}\,. \tag{48}$$

For convenience, we use the abbreviation $g^0 = g(|I^0 * \nabla G_\sigma|)$. (D) in (48) denotes the diffusion term, (A) the advection term and (F) the external force term. The term g^0 is called the edge detector. We can observe that value of the edge detector is approximately equal to zero close to image edges. Consequently, the evolution of the segmentation function slows down in the neighborhood of image edges. On the contrary, in parts of the image with constant intensity the edge detector equals to one. The advection term attracts the segmentation function to the image edges. We propose an advection parameter $\mathcal{A}$ to change the magnitude of the advection term and obtain the modified level set equation, namely

$$\partial_t u = g^0 |\nabla u|_\varepsilon \nabla \cdot \left(\frac{\nabla u}{|\nabla u|_\varepsilon} \right) + \mathcal{A} \nabla g^0 \cdot \nabla u - g^0 |\nabla u|_\varepsilon F\,. \tag{49}$$

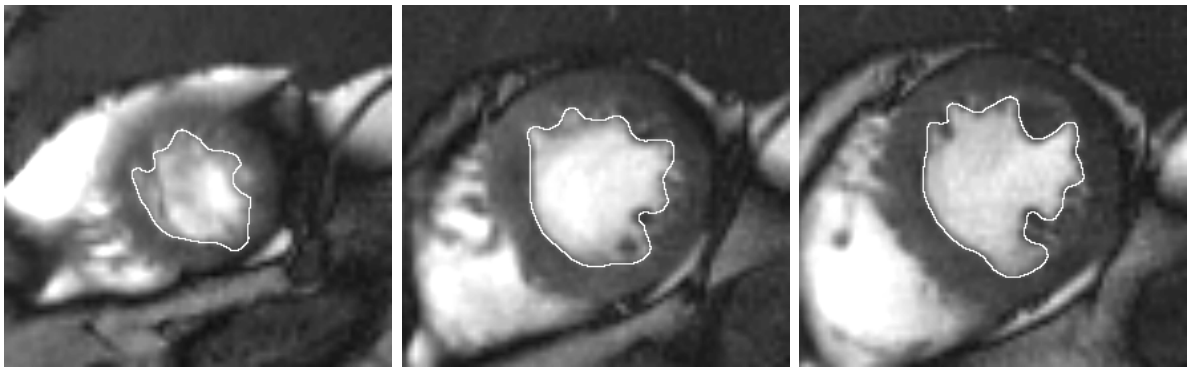

Figure 9: Segmentation result for three spatial slices at the end-diastole with parameters $h = 0.0028$, $\lambda = 0.25$, $\mathcal{A}_{\text{out}} = 2$, $F_{\text{out}} = -10$, $F_{\text{in}} = 50$.

Finally, using the zero Neumann boundary condition we define the following initial-boundary value problem

$$\begin{aligned}
\partial_t u(t,x) &= g^0 |\nabla u|_\varepsilon \nabla \cdot \left(\frac{\nabla u}{|\nabla u|_\varepsilon} \right) + \mathcal{A} \nabla g^0 \cdot \nabla u - g^0 |\nabla u|_\varepsilon F && \text{in } (0,T) \times \Omega\,, \\
u(0,x) &= d_{\Gamma_0}(x) && \text{in } \Omega\,, \\
\frac{\partial u}{\partial n}(t,x) &= 0 && \text{in } (0,T) \times \partial\Omega\,.
\end{aligned}$$

Numerical algorithm solving this problem is the key part of the segmentation algorithm.

A numerical scheme with justified key features such as stability and convergence can become a basis for a reliable and efficient algorithm. For this purpose, a semi-implicit co-volume space discretization is used. This approach is similar to [19], [20], [21], [42]. We choose a uniform discrete time step τ and approximate the time derivative in (49) by backward difference. The linear terms of the equation are considered at the current time level while the nonlinear terms (i.e. $|\nabla u|_\varepsilon$) are treated at the previous time level. In this way we obtain the following semi-implicit discretization

$$\frac{u^k - u^{k-1}}{\tau} = g^0 |\nabla u^{k-1}|_\varepsilon \nabla \cdot \left(\frac{\nabla u^k}{|\nabla u^{k-1}|_\varepsilon} \right) + \mathcal{A} \nabla g^0 \cdot \nabla u^k - g^0 |\nabla u^{k-1}|_\varepsilon F\,. \tag{50}$$

To simplify the construction of spatial discretization, we rewrite the previous equation using the following expression

$$g^0 \nabla \cdot \left(\frac{\nabla u^k}{|\nabla u^{k-1}|_\varepsilon} \right) = \nabla \cdot \left(g^0 \frac{\nabla u^k}{|\nabla u^{k-1}|_\varepsilon} \right) - \nabla g^0 \cdot \frac{\nabla u^k}{|\nabla u^{k-1}|_\varepsilon}\,. \tag{51}$$

Now we substitute (51) to (50). Dividing by $|\nabla u^{k-1}|_\varepsilon$, we get new form of (50)

$$\frac{1}{|\nabla u^{k-1}|_\varepsilon} \frac{u^k - u^{k-1}}{\tau} = \nabla \cdot \left(g^0 \frac{\nabla u^k}{|\nabla u^{k-1}|_\varepsilon} \right) + (\mathcal{A} - 1) \frac{1}{|\nabla u^{k-1}|_\varepsilon} \nabla g^0 \cdot \nabla u^k - g^0 F\,. \tag{52}$$

The co-volume method (see [37]) is used to construct a fully-discrete system of equation. Example of the algorithm function is shown in Figure 9.

3.4 Fractional advection-dispersion equation

The limited extent of this work did not leave much space to mention interesting results obtained for the multi-phase flow in porous media (e.g. see [29, 30, 31]), combustion (see e.g. [59, 58]) or turbulent transport of aerosols ([13, 36]).

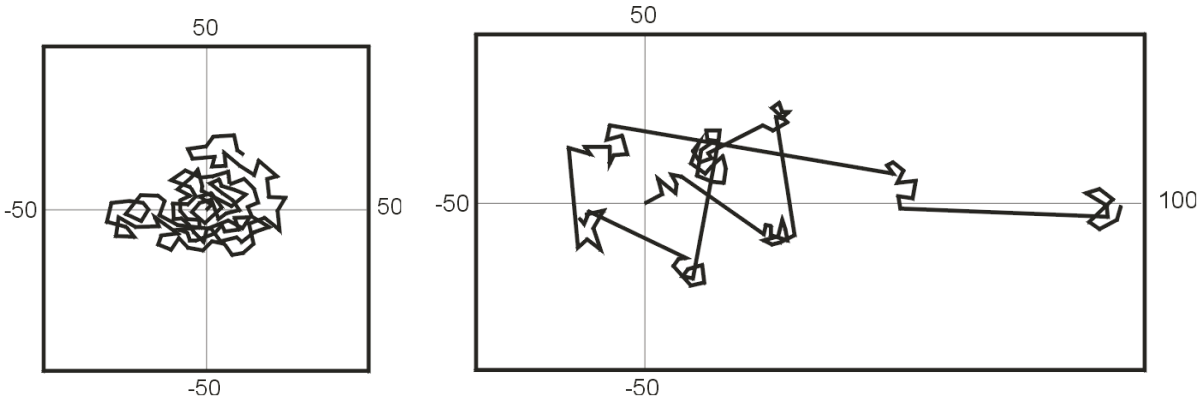

Figure 10: The Brownian motion schematically compared to the Lévy motion

Despite this fact, we mention a subject of ongoing research devoted to the anomalous transport in porous media described by the following equation in $\mathbb{R}^n$, $n = 1, 2, 3$

$$\frac{\partial u}{\partial t} + \mathbf{v} \cdot \nabla u = \Lambda \nabla_M^\alpha u + Q(t, x), \tag{53}$$

where $u = u(t, x)$ is the concentration (probability density), $\mathbf{v} = \mathbf{v}(t, x)$ the known velocity field, $\Lambda > 0$ the spread coefficient (dimensionally different from the usual diffusion coefficient), $M = M(\theta)$ the mixing measure on unit sphere (not necessarily symmetric), $\alpha \in (1, 2\rangle$ the fractional derivative order (the index of stability of Lévy motion - the measure of super-diffusivity, in other words), $Q = Q(t, x)$ the source term.

The generalized operator of fractional order is defined as

$$\nabla_M^\alpha f\,(x, t) = \frac{1}{\Gamma\,(-\alpha)} \int_{|\theta|=1} \int_0^\infty r^{-\alpha-1} f\,(x - r\theta, t)\, dr \cdot M\,(\theta)\, d\theta.$$

The equation delivered in [41] generalizes the advection-diffusion equation and allows to study the anomalous effects out of usual diffusion processes in porous media or distribution of atoms along surfaces.

In fact, the Brownian motion can be generalized to the Lévy motion (allowing for infinite invariance, the probability density is shifted toward the tails - see [14, 23] and Figure 10).

The preliminary computational studies showed promising behaviour of the solution when coupled to the Darcy flow in porous media as shown in [2, 10]. On the other hand, equation (53) is justified by the relation to stochastic processes only, and its meaning is still to be studied.

4 Outlook of the research and education in the given field

The presented topic of nonlinear diffusion is related to mathematical as well as applied research in the domains of chemical reactions, combustion, material science, flow in porous media, computer image processing and many others. Within the framework of the research carried at the Faculty of Nuclear Sciences and Physical Engineering of the Czech Technical University in Prague, the investigation can be focused on the following issues:

- phase transitions in multi-component materials at micro-scale (quantitatively accurate models of alloys solidification)

- surface diffusion in thin films and epitaxial growth (models incorporating elastic effects)
- multi-phase multi-component flow in porous media with phase changes (evaporation and freezing/thawing)
- nonlinear diffusion methods in image processing (processing algorithms for medical data with apriori known properties)
- advanced methods of high performance computing (parallelization and GPU computing of nonlinear diffusion)

The research is closely connected to the bachelor, master and Ph.D. theses of supervised students as well as to the contents of the courses, in the study branches Mathematical Engineering and Mathematical Informatics in particular. The following issues reflect the progress in the research of the nonlinear diffusion and applications:

- introducing new topics for the bachelor, master and Ph.D. theses
- introducing new courses reflecting the progress in the mathematics of nonlinear diffusion and continuum mechanics
- maintaining and broadening the international cooperation
- improving the industrial contacts

References

[1] R.J. Asaro and W.A. Tiller. Interface morphology development during stress corrosion cracking: Part I. Via surface diffusion. *Met. Trans.*, 3:1789–1796, 1972.

[2] P. Bednařík. Improved numerical method for multidirectional fractional advection-dispersion equation in 1-D and 2-D with general boundary condition. *COE Lecture Note*, 6:9–24, 2007.

[3] M. Beneš. Modelling of dendritic growth in pure substances. *Acta Techn. CSAV*, 39:375–397, 1994.

[4] M. Beneš. Anisotropic phase-field model with focused latent-heat release. In *FREE BOUNDARY PROBLEMS: Theory and Applications II*, pages 18–30, Chiba, Japan, 2000. GAKUTO International Series Mathematical Sciences and Applications, Vol.14.

[5] M. Beneš. Mathematical analysis of phase-field equations with numerically efficient coupling terms. *Interfaces and Free Boundaries*, 3, 2001. 201–221.

[6] M. Beneš. Mathematical and computational aspects of solidification of pure substances. *Acta Mathematica Universitatis Comenianae*, 70, No. 1:123–152, 2001.

[7] M. Beneš. Diffuse-interface treatment of the anisotropic mean-curvature flow. *Applications of Mathematics*, 48, No. 6:437–453, 2003.

[8] M. Beneš. Numerical solution for surface diffusion on graphs. *COE Lecture Note*, 3:9–25, 2006.

[9] M. Beneš. Computational studies of anisotropic diffuse interface model of microstructure formation in solidification. *Acta Mathematica Universitatis Comenianae*, 76 (1):35–50, 2009.

[10] M. Beneš. Numerical simulation of anomalous transport in porous media described by fractional-advection dispersion equation. SIAM Conference on Mathematical and Computational Issues in the Geosciences, Long Beach, 2011.

[11] M. Beneš, V. Chalupecký, and K. Mikula. Geometrical image segmentation by the Allen-Cahn equation. *Applied Numerical Mathematics*, 51, No. 2:187–205, 2004.

[12] M. Beneš, J. Kratochvíl, J. Křišťan, V. Minárik, and P. Pauš. A parametric simulation method for discrete dislocation dynamics. *European Phys. J. ST*, 177:177–192, 2009.

[13] M. Beneš and R.F. Holub. Aerosol wall deposition in enclosures investigated by means of a stagnant layer. *Environment International*, 22, Suppl. 1:S883–S889, 1996.

[14] D.A. Benson, S.W. Wheatcraft, and M.M. Meerschaert. Application of a fractional advection-dispersion equation. *Water Resources Research*, 36(6):1403–1412, 2000.

[15] H. Brezis. *Functional Analysis, Sobolev Spaces and Partial Differential Equations*. Springer Verlag, Berlin, 2010.

[16] G. Caginalp. An analysis of a phase field model of a free boundary. *Arch. Rational Mech. Anal.*, 92:205–245, 1986.

[17] F. Cao. *Geometric Curve Evolution and Image Processing*. Lecture Notes in Mathematics 1805, Springer Verlag, Berlin, 2003.

[18] R. Chabiniok and J. Tintěra. Cardiac MRI data segmentation using the partial differential equation of Allen-Cahn type. *COE Lecture Note*, 6:37–49, 2007.

[19] S. Corsaro, K. Mikula, A. Sarti, and F. Sgallari. Semi-implicit co-volume method in 3D image segmentation. *SIAM Journal on Scientific Computing*, 28, No. 6:2248–2265, 2006.

[20] A. Handlovičová and K. Mikula. Stability and consistency of the semi-implicit co-volume scheme for regularized mean curvature flow equation in level set formulation. *Applications of Mathematics*, 53, No. 2:105–129, 2008.

[21] A. Handlovičová, K. Mikula, and A. Sarti. Numerical solution of parabolic equations related to level set formulation of mean curvature flow. *Computing and Visualization in Science*, 1, No. 3:179–182, 1998.

[22] M.G. Crandall, H. Ishii, and P.-L. Lions. User's guide to viscosity solutions of second-order partial differential equations. *Bul. AMS*, 27:1–67, 1992.

[23] D.W. Dean, T.H. Illangasekare, and T.F. Russell. A stochastic differential equation approach for modeling of NAPL flow in heterogeneous porous media. UCD/CCM Report No. 225, Center for Computational Mathematics Reports, University of Colorado at Denver, 2005.

[24] B. Devincre and L.P. Kubin. Mesoscopic simulations of dislocations and plasticity. *Mater. Sci. Eng. A*, 8–14:234–236, 1997.

[25] F. Dkhil, E. Logak, and Y. Nishiura. Some analytical results on the Gray-Scott model. *Asymptotic Analysis*, 39:225–261, 2004.

[26] P. Dvořák. Mathematical modelling of microstructures in phase transitions. Master's thesis, Department of Mathematics, Faculty of Nuclear Sciences and Physical Engineering, Czech Technical University, 2010.

[27] L.C. Evans. *Partial Differential Equations*. American Mathematical Society, Providence, Rhode Island, 2010.

[28] L.C. Evans and J. Spruck. Motion of level sets by mean curvature I. *J. Diff. Geom.*, 33:635–681, 1991.

[29] R. Fučík, J. Mikyška, M. Beneš, and T.H. Illangasekare. An Improved Semi-Analytical Solution for Verification of Numerical Models of Two-Phase Flow in Porous Media. *Vadose Zone Journal*, 2007(6):93–104, June 2007.

[30] R. Fučík, J. Mikyška, M. Beneš, and T.H. Illangasekare. Semianalytical Solution for Two-Phase Flow in Porous Media with a Discontinuity. *Vadose Zone Journal*, 7(3):1001–1007, 8 2008.

[31] R. Fučík, J. Mikyška, T. Sakaki, M. Beneš, and TH Illangasekare. Significance of Dynamic Effect in Capillarity during Drainage Experiments in Layered Porous Media. *Vadose Zone Journal*, 9(9):697–708, AUG 2010.

[32] P. Gray and S.K. Scott. Autocatalytic reactions in the isothermal, continuous stirred tank reactor: oscillations and instabilities in the system $A + 2B \to 3B$, $B \to C$. *Chem. Eng. Sci.*, 39, No. 6:1087–1097, 1984.

[33] M. Gurtin. On the two-phase Stefan problem with interfacial energy and entropy. *Arch. Rational Mech. Anal.*, 96:200–240, 1986.

[34] M. Gurtin. *Thermomechanics of Evolving Phase Boundaries in the Plane*. Clarendon Press, Oxford, 1993.

[35] P. Habásko. Mathematical modelling of reaction-diffusion processes in combustion. Bachelor thesis, Department of Mathematics, Faculty of Nuclear Sciences and Physical Engineering, Czech Technical University, 2011.

[36] R.F. Holub, M. Beneš, and B.D. Honeyman. Interfacial phenomena in fluid dynamics: Linking atomistic and macroscopic properties: Can they explain the transport anomalies? In *Proceedings of Czech-Japanese Seminar in Applied Mathematics 2004, editors M. Beneš, J. Mikyška, T. Oberhuber*, pages 57–62, Prague, 2005. ISBN 80-01-03181-0.

[37] R. Máca, M. Beneš, and J. Tintěra. Application of a degenerate diffusion method in medical image processing. *Journal of Math-for-Industry*, 3:33–40, 2011.

[38] J. Mach. Application of the nonlinear Galerkin FEM method to the solution of the reaction diffusion equations. *Journal of Math-for-Industry*, 3:41–51, 2011.

[39] J. Mach. Numerical solution of the Gray-Scott reaction-diffusion system. Study of Ph.D. Thesis, 2011.

[40] J. Mach and M. Beneš. Nonlinear Galerkin FEM method to the solution of the reaction-diffusion equations. in preparation, 2012.

[41] M.M. Meerschaert, D.A. Benson, and B. Baumer. Multidimensional advection and fractional dispersion. *Physical Review E*, 59(5):5026–5028, 1999.

[42] K. Mikula, A. Sarti, and F. Sgallari. Co-volume level set method in subjective surface based medical image segmentation. In D.L. Wilson J.S. Suri and S. Laxminarayan, editors, *Handbook of Biomedical Image Analysis*, pages 583–626, New York, 2005.

[43] V. Minárik. *Mathematical Model of Discrete Dislocation Dynamics*. PhD thesis, Department of Mathematics, Faculty of Nuclear Sciences and Physical Engineering, Czech Technical University, 2009.

[44] V. Minárik, M. Beneš, and J. Kratochvíl. Simulation of dynamical interaction between dislocations and dipolar loops. *J. Appl. Phys.*, 107:061802, 2010.

[45] V. Minárik, J. Kratochvíl, K. Mikula, and M. Beneš. Numerical simulation of dislocation dynamics. In M. Feistauer, V. Dolejší, P. Knobloch, and K. Najzar, editors, *Numerical Mathematics and Advanced Applications, ENUMATH 2003 (peer reviewed proceedings)*, pages 631–641. Springer Verlag, 2004, ISBN 3-540-21460-7.

[46] W.W. Mullins. Theory of thermal grooving. *J. Appl. Phys.*, 28(3):333–339, 1957.

[47] W.W. Mullins. The effect of thermal grooving on grain boundary motion. *Acta Metall.*, 6:414–427, 1958.

[48] T.N. Narasimhan. Fourier's heat conduction equation: History, influence, and connections. *Reviews of Geophysics*, 37(1):151–172, 1999.

[49] Y. Nishiura and D. Ueyama. Self-replication, self-destruction, and spatio-temporal chaos in the Gray-Scott model. *Forma*, 15:281–289, 2000.

[50] S. Osher and R. Fedkiw. *Level Set Methods and Dynamic Implicit Surfaces*. Springer Verlag, New York, 2003.

[51] N. Paragios. Variational methods and partial differential equations in cardiac image analysis. In IEEE, editor, *Invited Publication : IEEE International Symposium on Biomedical Imaging: From Nano to Macro*, pages 17–20, Arlington, VA, USA, 2004.

[52] P. Perona and J. Malik. Scale space and edge detection using anisotropic diffusion. *IEEE Transactions on Pattern Analysis and Machine Intelligence*, 12, No. 7:629–639, 1990.

[53] G. Sapiro. *Geometric Partial Differential Equations and Image Processing*. Cambridge University Press, Cambridge, 2001.

[54] S.K. Scott, J. Wang, and K. Showalter. Modelling studies of spiral waves and target patterns in premixed flames. `http://www.rsc.org/ej/FT/1997/a608474e.pdf`, 1997.

[55] J. Šembera and M. Beneš. Nonlinear Galerkin method for reaction-diffusion systems admitting invariant regions. *Journal of Comp. and Appl. Math.*, 136, No. 1-2:163–176, 2001.

[56] J.A. Sethian. *Level Set Methods*. Cambridge University Press, New York, 1996.

[57] J. Smoller. *Shock Waves and Reaction-Diffusion Equations*. Springer Verlag, Berlin, 1993.

[58] R. Straka and M. Beneš. Numerical Simulation of NO production in Air-Staged Pulverized Coal Fired Furnace. *The Open Thermodynamics Journal*, 4:27–35, January 2010.

[59] R. Straka, J. Makovička, and M. Beneš. Numerical Simulation of NO Production in Pulverized Coal Fired Furnace. *Polish Journal of Environmental Studies*, 37(2):13–22, 2011.

[60] R. Temam. *Infinite-Dimensional Dynamical Systems in Mechanics and Physics*. Springer Verlag, New York, 1988.

[61] V. Tomica. Mathematical modelling of advection and reaction processes in combustion. Master's thesis, Department of Mathematics, Faculty of Nuclear Sciences and Physical Engineering, Czech Technical University, 2011.

[62] V. Tomica. Reaction-diffusion equations in combustion. to appear in COE Lecture Note, 2012.

[63] A. Visintin. *Models of Phase Transitions*. Birkhäuser, Boston, 1996.

[64] D. Ševčovič. Qualitative and quantitative aspects of curvature driven flows of planar curves. In P. Kaplický and Š. Nečasová, editors, *Topics on Partial Differential Equations*, pages 55–119. Lecture Notes Vol. 2, Jindřich Nečas Center for Mathematical Modelling, Faculty of Mathematics and Physics, Charles University in Prague, MatFyzPress, Prague, 2007.

Curriculum vitae

MICHAL BENEŠ

Education:
MSc. in Mathematical Engineering, Czech Technical University in Prague, 1989, Doctor of Technical Sciences, Czech Technical University in Prague, 1997
Positions:
Vice-Dean of the Faculty, since 2006
Vice-Head of the Department, since 2003
Associated Professor (Docent) in Applied Mathematics, Czech Technical University in Prague, since 2002
Assistant Professor, Czech Technical University in Prague, 1992-2002
PhD study, Czech Technical University in Prague, 1991-92
Study stay, Czech Technical University in Prague, 1989-91
Visiting positions:
Research stay in the Laboratoire de Métallurgie Physique, École Polytechnique Fédérale de Lausanne (Département des Matériaux), 1992-1993; Research stays in the US Bureau of Mines Denver (1994-5), in CINECA Bologna (2001), at the Kyushu University, Fukuoka (2002), at the Colorado School of Mines, Golden (regularly since 2000). Visiting Researcher UCLA Los Angeles (2006), Visiting Research Professor, Colorado School of Mines, Golden (since 2008).
Important research projects during past 5 years:
Principal investigator: Modern Methods of Mathematical Modelling and Numerical Simulation of Technological and Natural Processes, MŠMT, Czech-Slovak cooperation (STU Bratislava) No. 83, 2006-2007; Development and Validation of Porous Media Flow and Transport Models for Subsurface Environmental Application, MŠMT Kontakt ME878, 2006-2009, cooperation with the Colorado School of Mines, Golden; Multiphase Porous Media Flow and Transport Numerical Models for Subsurface Environmental Application, MŠMT Kontakt ME10009, 2010-2012, cooperation with the Colorado School of Mines, Golden; Two scales discrete-continuum approach to dislocation dynamics, Grant Agency of the Czech Republic P108/12/1463, 2012-2015.
Co-principal investigator: Jindřich Nečas Center for Mathematical Modelling, Research center MŠMT LC06052, 2006-2011; Applied Mathematics in Technical and Physical Sciences, Research Direction MŠMT 6840770010, 2005-2011; Advanced Methods in Control and Optimization of Energy Production, Ministry of Industry, 1H-PK/22, 2004-2008; Advanced control and optimization of biofuel combution in energy production, Technological Agency TAČR TA01020871, 2011-2013.
Impact of publications:
Web of Science: 14 articles, 52 citations, H-index: 4 (March 2011)
Supervising students:
16 bachelor theses, 27 master theses, 6 Ph.D. theses (by 2011)
Personal:
born October 5, 1965, married, 3 children